JOURNAL OF SYNCHROTRON RADIATION

ISSN 1600-5775

Received 18 October 2016
Accepted 15 February 2017

Edited by A. F. Craievich, University of São Paulo, Brazil

Keywords: rheology; pressure; small-angle X-ray scattering; complex solutions; hyaluronan.

Supporting information: this article has supporting information at journals.iucr.org/s

Complex solutions under shear and pressure: a rheometer setup for X-ray scattering experiments

D. C. F. Wieland,[a,b]* T. Zander,[a] V. M. Garamus,[a] C. Krywka,[a] A. Dedinaite,[c,d] P. Claesson[c,d] and R. Willumeit-Römer[a]

[a]Institute for Materials Research, Helmholtz Zentrum Geesthacht, Max-Planck-Strasse 1, Geesthacht 21502, Germany, [b]EMBL Hamburg, Notkestrasse 85, Hamburg 22607, Germany, [c]Department of Chemistry, Surface and Corrosion Science, KTH Royal Institute of Technology, Drottning Kristinas väg 51, Stockholm 10044, Sweden, and [d]SP Chemistry, Materials and Surfaces, SP Technical Research Institute of Sweden, Box 5607, Stockholm SE-114 86, Sweden. *Correspondence e-mail: florian.wieland@hzg.de

A newly developed high-pressure rheometer for *in situ* X-ray scattering experiments is described. A commercial rheometer was modified in such a way that X-ray scattering experiments can be performed under different pressures and shear. First experiments were carried out on hyaluronan, a ubiquitous biopolymer that is important for different functions in the body such as articular joint lubrication. The data hint at a decreased electrostatic interaction at higher pressure, presumably due to the increase of the dielectric constant of water by 3% and the decrease of the free volume at 300 bar.

1. Introduction

The viscous and elastic properties of fluids are determined by their molecular structure, intermolecular interactions and by external factors such as temperature and pressure (Seeton, 2006; Mezger, 2011). These properties might be easily scaled for single-phase systems, *e.g.* the viscosity increases when the temperature is decreased. However, the situation is more complex in multicomponent systems such as aqueous solutions of micelles or polymers. In such systems, the ingredients interact and their organization may be affected by shearing, giving rise to rheological effects such as shear thinning, shear thickening or shear banding (Helgeson *et al.*, 2009; Eberle *et al.*, 2014; Mezger, 2011). One parameter that is of interest in this context is the influence of pressure on the viscoelastic properties of the sample due to its effect on the inter- and intramolecular interactions. It is of importance to elucidate how external parameters affect rheological properties in different scientific fields where complex fluids are exposed to shear and pressure. Examples include the processing of food (extrusion, high-speed blending, homogenization) and its final texture and sensory experience whilst chewing (Totten & Negri, 2012; Oey *et al.*, 2008), achieving high infiltration and efficiency of liquid media for enhanced oil recovery methods (pressures from 200 to 1000 bar) (Mitchell *et al.*, 2016; Clarke *et al.*, 2015; Lake, 1989), and the functionality of the lubrication systems in the human body (Klein, 2006). Insight can be gained by elucidating the structural changes of multicomponent systems *in situ* at different shear rates and pressure conditions. X-ray scattering techniques allow the exploration of the structural properties of such multicomponent systems in different sample environments without disturbing the sample. Experiments combining rheometry and scattering have been successfully applied to study stable and flocculated colloidal

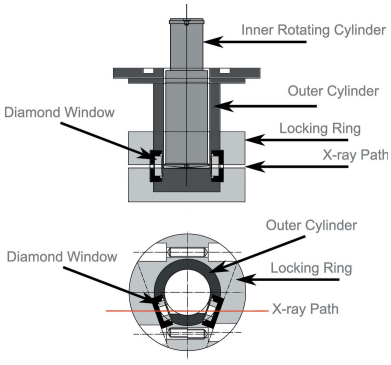

suspensions (Pignon *et al.*, 1997; Jogun & Zukoski, 1999; Versmold *et al.*, 2001; Panine *et al.*, 2002; Hoekstra *et al.*, 2005), surfactant systems (Diat *et al.*, 1993; Roux *et al.*, 1995; Molino *et al.*, 1998; With *et al.*, 2014), liquid crystalline systems (Hongladarom *et al.*, 1996; Burghardt, 1998; Hoekstra *et al.*, 2002; Cinader & Burghardt, 1999), flow-enhanced crystallization in polymers (Kumaraswamy *et al.*, 2004; Agarwal *et al.*, 2003; Somani *et al.*, 2000; Liu *et al.*, 2011), polymer nanocomposites (Pujari *et al.*, 2011; Dykes *et al.*, 2012), and the effect of shear on shape, orientation and size of individual objects (Trebbin *et al.*, 2013; Wieland, Garamus *et al.*, 2016). However, different setups exist which allow the investigation of structural changes under high hydrostatic pressure ranging from ambient to several MPa (Wirkert *et al.*, 2014; Krywka *et al.*, 2008; Kohlbrecher *et al.*, 2007; Castelletto *et al.*, 2008; Yang *et al.*, 2016).

The existing rheometry setups allow the investigation of the structure and viscosity as functions of shear rate and temperature. However, to the best of the authors' knowledge, up to now there has been no rheometer setup that also allows changing the hydrostatic pressure in the solution under consideration. We have developed an X-ray scattering setup which allows the control of temperature, shear rate and hydrostatic pressure, and the investigation of the *in situ* macromolecular and solution structures. We utilize a commercial rheometer with a pressure cell that has been modified to allow X-ray scattering experiments.

The development of the setup was triggered by a need to gain insight into the remarkable lubrication system in the articular joint, which provides extremely low friction forces (friction coefficient of the order of 0.001) under various conditions. The shear rates can reach values of up to 10^6 s^{-1} and pressures of 150 bar (15 MPa) are reported during everyday activities (Klein, 2006; Hodge *et al.*, 1986; Morrell *et al.*, 2005; Afoke *et al.*, 1987). The articular joint also has a surprisingly high wear resistance, considering the fragile structure of cartilage, as it often works for our entire life. Clearly, different components such as proteins, biopolymers, lipids and other macromolecules interact to form a highly efficient lubrication system with respect to wear, flexibility and low friction values (Lee & Spencer, 2008; Liu *et al.*, 2012; Dėdinaitė, 2012; Schmidt *et al.*, 2007; Chang *et al.*, 2009; Zappone *et al.*, 2007; Coles *et al.*, 2010; Nitzan *et al.*, 2001; Serro *et al.*, 2006). The components of the synovial fluid are likely to adapt to different loads and shear conditions by re-structuring and, thereby, provide extremely low friction coefficients under different pressures and shear rate conditions (Lee & Spencer, 2008). The self-assembly of the components promoting lubrication, as well as how this may lead to lubrication synergy, is not sufficiently understood, even though some progress has been made in recent years (Seror *et al.*, 2012, 2011; Klein, 2006; Wang *et al.*, 2015, 2013 ; Wieland, Degen *et al.*, 2016; Zander *et al.*, 2016; Dėdinaitė, 2012). For example, investigations show that hyaluronic and albumin form complexes that can result in rheopexy behaviour of the mixed solutions under physiological conditions, which influences the mechanical properties of the synovial fluid (Oates *et al.*, 2006; Lenormand *et al.*, 2008).

The biopolymer hyaluronan is an essential part of the extracellular matrix and fulfils many different functions (Necas *et al.*, 2008; Almond, 2007). The linear polysaccharide is built of disaccharide units which are repeated along the chain. The main interaction possibilities for hyaluronan are hydrogen bonding *via* OH groups, hydrophobic interactions *via* non-polar patches in the chain and electrostatic interaction due to the presence of one carboxylate group on each disaccharide subunit (Milas & Rinaudo, 1998; Scott & Heatley, 1999; Necas *et al.*, 2008). Hyaluronan is described as a semi-flexible anionic polyelectrolyte (Villetti *et al.*, 2000; Salamon *et al.*, 2013). The typical polyelectrolyte correlation peak that occurs in many scattering studies of polyelectrolyte solutions is hard to observe in hyaluronan solutions and only appears as a shoulder. The origin of this correlation peak is due to the electrostatic repulsion between the hyaluronan chains (De Gennes, 1979; De Gennes *et al.*, 1976). The peak shifts as a function of the concentration to higher-q values as the distance between the single chains is decreased, which is the typical behaviour of the polyelectrolyte solution (DeSmedt *et al.*, 1994). Rheological investigations combined with small-angle X-ray scattering have demonstrated an enhancement of this polyelectrolyte peak by applying shear (Villetti *et al.*, 2000). This increase can be seen as a decrease in the fluctuation of the separation between hyaluronan chains by shear. Thus, the strength of the correlation peak increases.

An increase in hydrostatic pressure results in different effects. First, the decrease of the free internal volume leads to ordering of solute and solvent molecules, which is a result of Le Chatelier's principle (Mozhaev *et al.*, 1996). An increased pressure also leads to destabilization of ion pairs and ionic interactions due to the effect of electrostriction at elevated pressures (Mozhaev *et al.*, 1996; Gross & Jaenicke, 1994). Furthermore, the exposure of hydrophobic groups to water is postulated to increase under pressure, which disturbs the dynamic structure of water. This promotes the formation of a hydrophobic solvation layer, which is more densely packed than bulk water (Kauzmann, 1959; Gross & Jaenicke, 1994; Hummer *et al.*, 1998; Schroer *et al.*, 2011). As hyaluronan has electrostatic and hydrophobic interaction sites, the question arises if and how the structural arrangement changes at elevated pressures. Here, we aim to find an answer to this question by exploring the structural changes of hyaluronan at elevated pressures under shear. We have conducted small-angle X-ray scattering experiments at shear rates ranging from 0 s^{-1} up to 1500 s^{-1} in a pressure range from 1 bar to 300 bar. As samples we chose aqueous hyaluronan solutions in the absence and the presence of 150 mM NaCl. Thus, we have one sample series with strong electrostatic interactions and a sample series where electrostatic interactions are effectively screened.

2. Rheometer design and setup

We have developed a setup for investigating complex fluids under shear forces and hydrostatic pressure. The setup allows simultaneous probing of the rheological response and the

structure of the sample as a function of pressure and shear rate. The basis of the setup is formed from a commercially available rheometer; we used the CV100 manufactured by Malvern, UK. The setup also includes a temperature-controlled pressure cell (HPC300, also from Malvern, UK). This measuring cell allows rheological measurements in cuvette geometry up to pressures of 300 bar. The accessible temperature range is from 1°C to 80°C. The cell material is Hastelloy, which prevents transmission of X-rays. The cell was, therefore, modified to allow simultaneous X-ray scattering experiments by adding X-ray transparent 500 µm-thick diamond windows. A sketch of the cell is shown in Fig. 1. In the standard design, the inner rotating cylinder has a sapphire bearing located at the bottom of the cylinder and supported on a ruby ball. The inner cylinder is connected to the rheometer by a magnetic ball. This part and the ability to measure viscosity curves are unaltered in our modified device. In order to meet the geometrical constraints and to maintain the pressure stability, a compromise had to be found for the location of the diamond windows. In existing rheometer setups, which are not able to apply pressure to the sample, a cuvette cell is used. Here, experiments are normally performed at two positions, where one is at the centre of rotation of the inner cylinder (radial geometry) and the other position is located at the gap between the inner and outer cylinder wall (tangential). None of these positions were usable for our setup, as the radial position is blocked by the inner rotating cylinder made of Hastelloy. It is not possible to change the material for this part as it needs to sustain the pressure. The tangential position is also not accessible as for this location the windows would have had to be mounted at a position where the pressure stability could not be maintained.

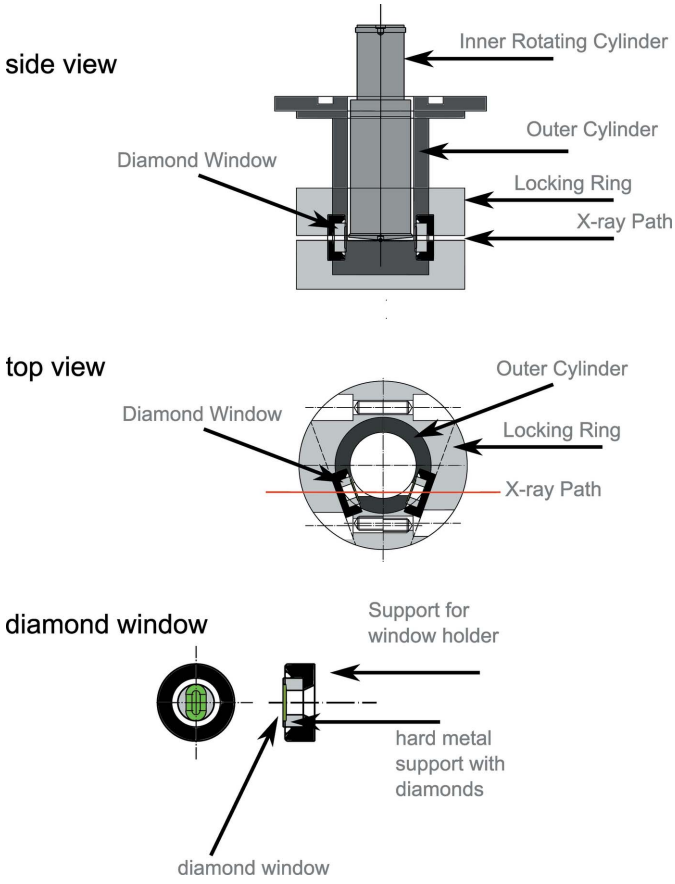

Figure 1
Sketch of the rheometer pressure cell for X-ray scattering experiments. The cell is modified to allow the X-ray beam to pass through the cell between the lower bottom and the inner rotating cylinder. The diamond windows are marked in green. The inner rotating cylinder has an angle of 5° with respect to the bottom plate, realising a cone-plate geometry. Not shown is the CV100 rheometer and the lid of the HPC300 pressure cell.

Instead we use the gap between the inner cylinder and the bottom of the pressure vessel. In order to have a well defined shear rate distribution at this position, the inner cylinder was modified to have a cone of 5° at the bottom of the cell. Thus, cone-plate geometry was achieved between the bottom of the pressure vessel and the cone end of the inner cylinder. The advantage of the cone-plate geometry is the independence of the shear rate on the radius and this allows X-ray experiments to be performed in this gap under well defined conditions. In this cone-plate geometry the radial position (where the X-ray beam travels through the centre of rotation) is not accessible because the ruby bearing blocks it. Therefore, the measuring position was chosen to have a maximum distance to the centre in order to have mainly tangential velocity components. In the supporting information, a histogram of the angular distribution of the velocity vectors with respect to the X-ray beam is shown in Fig. S1, and Fig. S2 presents a visualization of the flow lines.

The X-ray path was 11 mm away from the axis of the cylinder, which has a radius of 13.5 mm. Polycrystalline diamonds were purchased from ElementSix, Luxembourg, produced *via* chemical vapour deposition. The diamonds were brazed in a hard metal fitting. A locking ring, which was tightened by eight screws, held them in position. Additionally, an O-ring was placed between the windows and the outer cylinder for proper sealing. The opening of the X-ray transparent windows was 2 mm × 6 mm with a radius of 2.5 mm at the corners; see Fig. 1, showing a sketch of the diamond window (marked by the green area). The resulting accessible scattering angles are 17.11° in the horizontal direction (parallel to the flow direction) and 5° in the direction perpendicular to the flow field, which is limited by the angle of the cone. Thus, the setup also allows wide-angle X-ray scattering (WAXS) measurements. The cone opening was a compromise to meet the requirement on the accessible angle for scattering experiments and rheological constraints. In this configuration shear rates from 0 s^{-1} up to 1500 s^{-1} can be reached in the lower gap. The total X-ray path length is 2.4 cm of sample volume and an additional 1 mm of diamond. Thus, high X-ray energies are optimal for this cell. In the first experiments, transmissions of ∼70% and ∼8% at 20 keV for the empty cell with diamond windows and filled with water, respectively, were observed, in good agreement with the theoretically calculated values of 71% and 8.5%. The pressure of the HPC300 is controlled *via* a hydrostatic pressure system manufactured by Sitec, Switzerland. The system consists of a hand pump that is able to generate pressures up to 4 kbar and

valves that separate the cell from the pump. In order to avoid mixing of the pressure medium and the sample in the cell, a special separator was manufactured. This separator consists of a honed tube with a moveable piston inside and offers a reservoir of 5 ml for the sample solution. Furthermore, the system is equipped with two pressure sensors (KGT, Kramer, Germany) that are sensitive to a pressure range from 0 bar to 500 bar. In order to control the pressure in the cell, one sensor is placed before the separator (between pump and separator) and the other one after.

3. Experimental

Hyaluronan (HA) was purchased from CreativePeg Works, USA, and had an average molecular weight of 750 kDa (Lot.: LZG11021801). Sodium chloride (assay >99.9%, catalogue No. HN00.1) was purchased from Carl Roth and HEPES (assay >99.5%, catalogue No. H3375) was obtained from Sigma-Aldrich. The HA samples were prepared under two different solution conditions, one without any salt present and the other with 150 m*M* NaCl and 20 m*M* HEPES buffer. The HA concentration was 8 mg ml^{-1} for all experiments. The water used in all experiments was purified using a Millipore system and had a resistivity of 18 MΩ cm at 25°C.

Measurements were performed at ID02, ESRF, Grenoble, France, and at P12 BioSAXS, Petra III, EMBL/DESY, Hamburg, Germany (Blanchet *et al.*, 2015). At the ID02 beamline, an energy of 18.5 keV was used, whereas at the BioSAXS beamline an energy of 20 keV was used. This high X-ray energy was necessary in order to have sufficient transmission. The accessible q range at the two beamlines was 0.1 nm^{-1} to 3 nm^{-1}, and 0.1 nm^{-1} to 6 nm^{-1}, respectively. The samples were measured at pressures of 1 bar, 200 bar and 300 bar. A table of the shear rates used at every pressure point is given in the supporting information; the lowest shear rate was 0 s^{-1} and the highest was 1500 s^{-1}.

4. Results

We will first discuss the effect of shear on the structure of HA in solutions without added salt at different pressures. Fig. 2 shows the scattering at 1 bar, 200 bar and 300 bar at zero shear rate. Due to the chosen solution conditions a broad polyelectrolyte correlation peak is visible at q = 0.3–0.5 nm^{-1}, which results from the electrostatic repulsion of the carboxylate groups of the HA chains. By increasing the pressure a decrease of the overall scattering intensity occurs, see Fig. 2. However, this effect can be attributed to a change in the scattering contrast. In Fig. S3 (supporting information), the curves for 1 bar and 300 bar are scaled to each other by a factor of 1.1. The resulting peaks show no structural difference, underlining that this change is just caused by the pressure dependence of the contrast. The data show a slight change in the upturn at low q, which consist in total of four data points. This and the fact that these data points are close to the beamstop make an interpretation difficult. This behaviour

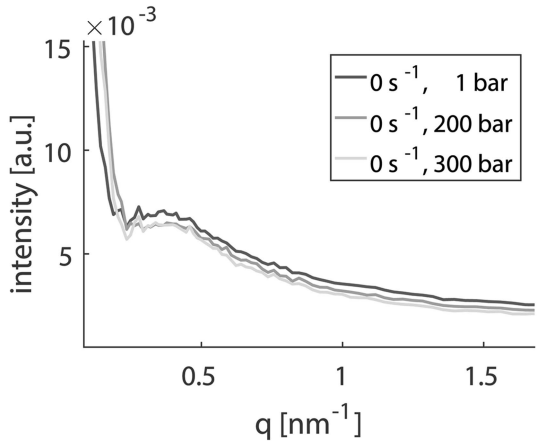

Figure 2
Radial-averaged scattering patterns of hyaluronan (8 mg ml^{-1}) without added salt at different pressures.

might indicate a change in the polymer conformation but for a solid statement a larger range at low q is necessary.

We investigated the HA solutions without salt at different pressures, ranging from 1 bar up to 300 bar, at different shear rates. The obtained scattering patterns for 1 bar (ambient conditions) and 300 bar are shown in Fig. 3. The two-dimensional scattering patterns showed no anisotropy. This is a result of the geometry of the rheometer as the X-ray beam travels parallel to the velocity field and, thus, is not sensitive to

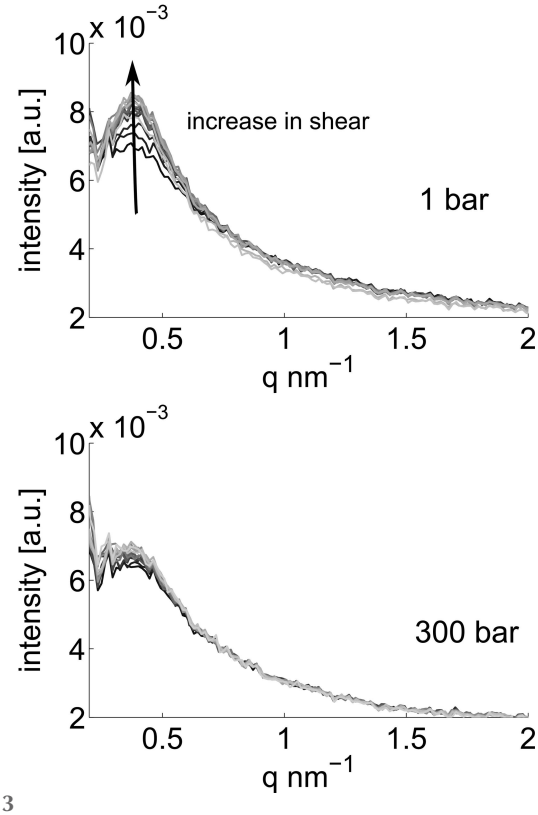

Figure 3
Radial-averaged scattering patterns of aqueous hyaluronan solutions (8 mg ml^{-1}) without added salt at different shear rates and pressures. The colour of the curves changes with the shear rate where black corresponds to 0 s^{-1} and light grey to 1500 s^{-1}.

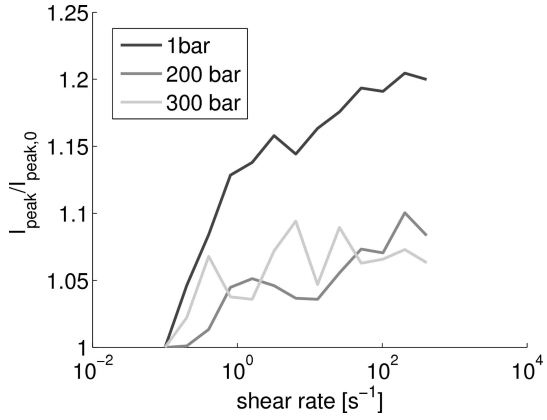

Figure 4
Comparison of the maximum of the polyelectrolyte peak as a function of the shear rate for HA solutions with a concentration of 8 mg ml^{-1} without added salt at three different pressures. The intensity at a given shear rate was normalized by that at zero shear rate to account for contrast changes due to the increased pressure and, thereby, facilitate comparison between the three curves.

shear-induced alignment. At 1 bar, the polyelectrolyte peak gains intensity with increasing shear rate up to 1500 s^{-1}, consistent with the data reported by Villetti *et al.* (2000) and attributed to an ordering effect. With increasing shear forces the fluctuations in the separation between the HA chain are decreased and, thus, the preferential separation between scattering units is more pronounced which is manifested by the stronger polyelectrolyte peak. As the q range is limited to 0.1 nm^{-1}, no information on the single-chain structure can be obtained. In contrast to ambient pressure conditions, the peak is not strongly affected by the shear rate at 300 bar, and only a slight increase in the peak intensity can be observed as the shear rate is increased from 0 to 1500 s^{-1}. In Fig. 4, the maximum peak intensity is plotted as a function of the shear rate for three different pressures. We have normalized the intensity of the peak by the intensity at zero shear rate at the respective pressure value. This was carried out in order to account for contrast changes due to the pressure increase. The not normalized data are shown in Fig. S4 of the supporting information. In order to extract the maximum peak intensity and position, a Gaussian function was fitted to the data on a linear scale. We note that the parameters obtained by this procedure have a maximum error of 0.02 nm^{-1} in position due to the wide nature of the polyelectrolyte peak. Clearly, the peak intensity at constant pressure increases with increasing shear rate. However, the increase in pressure reduces this trend compared with the data at 1 bar. The position of the peak found in our 8 mg ml^{-1} HA solution does not show any shift and stays constant at 0.35 ± 0.02 nm^{-1} indicating no change in the preferential distance between the scattering objects which is roughly $D = 2\pi/q_{peak} = 18$ nm. In the study by Villetti *et al.* (2000), the correlation peak was found to be located at 0.57 nm^{-1}, a shift that is consistent with the higher HA concentration of 15 mg ml^{-1} used by them.

In order to test the hypothesis of an increase of the electrostatic interaction by a shear rate driven alignment, we have repeated the measurements with HA and 150 mM added salt; thus, screening the electrostatic interactions. Fig. S5 shows the scattering curves obtained at different shear rates and pressures with added salt. Here, no effect of shear rate can be observed. The slight changes are likely due to an increase of the scattering background with pressure, which can be attributed to the changed scattering contrast.

5. Discussion

In this experiment we have investigated the structural organization of aqueous solutions of the biopolymer hyaluronan as a function of pressure and shear rate. We find that the characteristic polyelectrolyte correlation peak increases in intensity with increasing shear rate. Thus, the characteristic distance between HA chains becomes more defined as fluctuations of the HA chain are decreased due to shear forces (Villetti *et al.*, 2000). At elevated pressures of 300 bar the increase of the peak intensity as a function of shear rate is less pronounced than at ambient pressure. The peak position does not change with pressure or shear rate, which suggests no change in the preferential distance between the HA chains. We note that in investigations over large pressure intervals some change of the scattering contrast occurs. We have, therefore, scaled the scattering curves at different pressures and with such a scaling the peak shows no significant change, underlining that the decrease in its intensity with increasing pressure at zero shear rate is only due to the lowered contrast.

The observation that the increase in the polyelectrolyte peak with increasing shear rate is more pronounced at lower pressures, and the fact that the position of the polyelectrolyte peak is not changed, suggest no change in the characteristic distance between the HA chains but a change in the interaction strength. As the intensity of the polyelectrolyte peak scales with the electrostatic interaction, the increase in dielectric constant of water with pressure could contribute to this observation (Floriano & Nascimento, 2004). Using the formulae from the cited paper, the relative change of the dielectric constant is 3% by an increase in the pressure to 300 bar, which seems to be too small to be the only origin of the effect. Another possible cause could be the decreased free volume, which might reduce fluctuations of the system and, thus, diminish the shear-induced increase of the structure factor peak. Clearly, more studies of the pressure and the temperature effects will be needed to shed further light on this issue.

6. Conclusions

We have constructed and tested a new rheometer setup that allows the investigation of the structural changes in solutions under shear as functions of pressure and temperature. The setup allows probing the structural rearrangement of polymers, proteins and complex mixtures in the shear range from 0 s^{-1} to 1500 s^{-1} at pressures from ambient up to 300 bar. Our data show an increase in the polyelectrolyte correlation peak in HA solutions in the absence of added salt with increasing

shear rate, particularly at low pressures. We attribute this to a shear-force-induced decrease of the fluctuations in the distance between the scattering objects. Further, under high shear conditions we observe a decrease in the electrostatic interactions with pressure, which can probably be attributed to an increase in the dielectric constant and a decrease of the free volume.

Acknowledgements

We wish to acknowledge the financial support by the BMBF-project 05K2012 within the Joint International Research Project Röntgen-Angström-Cluster. We acknowledge Johannes Möller from the ID02, ESRF, France, for support during beam time. Further, we thank Martin Schroer and Felix Lehmkühler for logistical help.

References

Afoke, N. Y. P., Byers, P. D. & Hutton, W. C. (1987). *J. Bone Joint Surg. Br.* **69**, 536–541.
Agarwal, P. K., Somani, R. H., Weng, W. Q., Mehta, A., Yang, L., Ran, S. F., Liu, L. Z. & Hsiao, B. S. (2003). *Macromolecules*, **36**, 5226–5235.
Almond, A. (2007). *Cell. Mol. Life Sci.* **64**, 1591–1596.
Blanchet, C. E., Spilotros, A., Schwemmer, F., Graewert, M. A., Kikhney, A., Jeffries, C. M., Franke, D., Mark, D., Zengerle, R., Cipriani, F., Fiedler, S., Roessle, M. & Svergun, D. I. (2015). *J. Appl. Cryst.* **48**, 431–443.
Burghardt, W. R. (1998). *Macromol. Chem. Phys.* **199**, 471–488.
Castelletto, V., Newby, G. E., Hamley, I. W., Noirez, L. & Baroni, P. (2008). *Langmuir*, **24**, 8319–8324.
Chang, D. P., Abu-Lail, N. I., Coles, J. M., Guilak, F., Jay, G. D. & Zauscher, S. (2009). *Soft Matter*, **5**, 3438–3445.
Cinader, D. K. & Burghardt, W. R. (1999). *Polymer*, **40**, 4169–4180.
Clarke, A., Howe, A. M., Mitchell, J., Staniland, J., Hawkes, L. & Leeper, K. (2015). *Soft Matter*, **11**, 3536–3541.
Coles, J. M., Chang, D. P. & Zauscher, S. (2010). *Curr. Opin. Colloid Interface Sci.* **15**, 406–416.
Dėdinaitė, A. (2012). *Soft Matter*, **8**, 273–284.
De Gennes, P. G. (1979). *Scaling Concepts in Polymer Physics*. Ithaca: Cornell University Press.
De Gennes, P. G., Pincus, P., Velasco, R. M. & Brochard, F. (1979). *J. Phys. Fr.* **37**, 1461–1473.
De Smedt, S. C., Lauwers, A., Demeester, J., Engelborghs, Y., De Mey, G. & Du, M. (1994). *Macromolecules*, **27**, 141–146.
Diat, O., Roux, D. & Nallet, F. (1993). *J. Phys. IV*, **3**, 193–204.
Dykes, L. M. C., Torkelson, J. M. & Burghardt, W. R. (2012). *Macromolecules*, **45**, 1622–1630.
Eberle, A. P. R., Martys, N., Porcar, L., Kline, S. R., George, W. L., Kim, J. M., Butler, P. D. & Wagner, N. J. (2014). *Phys. Rev. E*, **89**, 050302(R).
Floriano, W. B. & Nascimento, M. A. C. (2004). *Braz. J. Phys.* **34**, 38–41.
Gross, M. & Jaenicke, R. (1994). *Eur. J. Biochem.* **221**, 617–630.
Helgeson, M. E., Reichert, M. D., Hu, Y. T. & Wagner, N. J. (2009). *Soft Matter*, **5**, 3858–3869.
Hodge, W. A., Fijan, R. S., Carlson, K. L., Burgess, R. G., Harris, W. H. & Mann, R. W. (1986). *Proc. Natl Acad. Sci. USA*, **83**, 2879–2883.
Hoekstra, H., Mewis, J., Narayanan, T. & Vermant, J. (2005). *Langmuir*, **21**, 11017–11025.
Hoekstra, H., Vermant, J., Mewis, J. & Narayanan, T. (2002). *Langmuir*, **18**, 5695–5703.
Hongladarom, K., Ugaz, V. M., Cinader, D. K., Burghardt, W. R., Quintana, J. P., Hsiao, B. S., Dadmun, M. D., Hamilton, W. A. & Butler, P. D. (1996). *Macromolecules*, **29**, 5346–5355.
Hummer, G., Garde, S., Garcia, A. E., Paulaitis, M. E. & Pratt, L. R. (1998). *Proc. Natl Acad. Sci. USA*, **95**, 1552–1555.
Jogun, S. M. & Zukoski, C. F. (1999). *J. Rheol.* **43**, 847–871.
Kauzmann, W. (1959). *Adv. Protein Chem.* **14**, 1–63.
Klein, J. (2006). *Proc. Inst. Mech. Eng. J. J. Eng. Tribol.* **220**, 691–710.
Kohlbrecher, J., Bollhalder, A., Vavrin, R. & Meier, G. (2007). *Rev. Sci. Instrum.* **78**, 125101.
Krywka, C., Sternemann, C., Paulus, M., Tolan, M., Royer, C. & Winter, R. (2008). *ChemPhysChem*, **9**, 2809–2815.
Kumaraswamy, G., Verma, R. K., Kornfield, J. A., Yeh, F. J. & Hsiao, B. S. (2004). *Macromolecules*, **37**, 9005–9017.
Lake, L. W. (1989). *Enhanced Oil Recovery*. Englewood Cliffs: Prentice-Hall.
Lee, S. & Spencer, N. D. (2008). *Science*, **319**, 575–576.
Lenormand, H., Deschrevel, B., Tranchepain, F. & Vincent, J. C. (2008). *Biopolymers*, **89**, 1088–1103.
Liu, C., Wang, M., An, J. X., Thormann, E. & Dėdinaitė, A. (2012). *Soft Matter*, **8**, 10241–10244.
Liu, Y. P., Zhou, W. Q., Cui, K. P., Tian, N., Wang, X., Liu, L. B., Li, L. B. & Zhou, Y. G. (2011). *Rev. Sci. Instrum.* **82**, 045104.
Mezger, T. G. (2011). *The Rheology Handbook*, 3rd ed. Hanover: Vincentz Network.
Milas, M. & Rinaudo, M. (1998). *Polysaccharides: Structural Diversity and Functional Versatility*, pp. 535–550. Boca Raton: CRC Press.
Mitchell, J., Lyons, K., Howe, A. M. & Clarke, A. (2016). *Soft Matter*, **12**, 460–468.
Molino, F. R., Berret, J. F., Porte, G., Diat, O. & Lindner, P. (1998). *Eur. Phys. J. B*, **3**, 59–72.
Morrell, K. C., Hodge, W. A., Krebs, D. E. & Mann, R. W. (2005). *Proc. Natl Acad. Sci. USA*, **102**, 14819–14824.
Mozhaev, V. V., Heremans, K., Frank, J., Masson, P. & Balny, C. (1996). *Proteins Struct. Funct. Genet.* **24**, 81–91.
Necas, J., Bartosikova, L., Brauner, P. & Kolar, J. (2008). *Vet. Med. Prague*, **53**, 397–411.
Nitzan, D. W., Nitzan, U., Dan, P. & Yedgar, S. (2001). *Rheumatology*, **40**, 336–340.
Oates, K. M. N., Krause, W. E., Jones, R. L. & Colby, R. H. (2006). *J. R. Soc. Interface*, **3**, 167–174.
Oey, I., Lille, M., Van Loey, A. & Hendrickx, M. (2008). *Trends Food Sci. Technol.* **19**, 320–328.
Panine, P., Narayanan, T., Vermant, J. & Mewis, J. (2002). *Phys. Rev. E*, **66**, 022401.
Pignon, F., Magnin, A., Piau, J. M., Cabane, B., Lindner, P. & Diat, O. (1997). *Phys. Rev. E*, **56**, 3281–3289.
Pujari, S., Dougherty, L., Mobuchon, C., Carreau, P. J., Heuzey, M. C. & Burghardt, W. R. (2011). *Rheol. Acta*, **50**, 3–16.
Roux, D. C., Berret, J. F., Porte, G., Peuvrel-Disdier, E. & Lindner, P. (1995). *Macromolecules*, **28**, 1681–1687.
Salamon, K., Aumiller, D., Pabst, G. & Vuletic, T. (2013). *Eur. Biophys. J.* **42**, S105.
Schmidt, T. A., Gastelum, N. S., Nguyen, Q. T., Schumacher, B. L. & Sah, R. L. (2007). *Arthritis Rheum.* **56**, 882–891.
Schroer, M. A., Zhai, Y., Wieland, D. C. F., Sahle, C. J., Nase, J., Paulus, M., Tolan, M. & Winter, R. (2011). *Angew. Chem. Int. Ed.* **50**, 11413–11416.
Scott, J. E. & Heatley, F. (1999). *Proc. Natl Acad. Sci. USA*, **96**, 4850–4855.
Seeton, C. J. (2006). *Tribol. Lett.* **22**, 67–78.
Seror, J., Merkher, Y., Kampf, N., Collinson, L., Day, A. J., Maroudas, A. & Klein, J. (2011). *Biomacromolecules*, **12**, 3432–3443.
Seror, J., Merkher, Y., Kampf, N., Collinson, L., Day, A. J., Maroudas, A. & Klein, J. (2012). *Biomacromolecules*, **13**, 3823–3832.

Serro, A. P., Gispert, M. P., Martins, M. C., Brogueira, P., Colaço, R. & Saramago, B. (2006). *J. Biomed. Mater. Res.* **78A**, 581–589.
Somani, R. H., Hsiao, B. S., Nogales, A., Srinivas, S., Tsou, A. H., Sics, I., Balta-Calleja, F. J. & Ezquerra, T. A. (2000). *Macromolecules*, **33**, 9385–9394.
Totten, G. E. & De Negri, V. J. (2012). *Handbook of Hydraulic Fluid Technology*. London: CRC Press.
Trebbin, M., Steinhauser, D., Perlich, J., Buffet, A., Roth, S. V., Zimmermann, W., Thiele, J. & Forster, S. (2013). *Proc. Natl Acad. Sci. USA*, **110**, 6706–6711.
Versmold, H., Musa, S., Dux, C., Lindner, P. & Urban, V. (2001). *Langmuir*, **17**, 6812–6815.
Villetti, M., Borsali, R., Diat, O., Soldi, V. & Fukada, K. (2000). *Macromolecules*, **33**, 9418–9422.
Wang, M., Liu, C., Thormann, E. & Dėdinaitė, A. (2013). *Biomacromolecules*, **14**, 4198–4206.
Wang, M., Zander, T., Liu, X. Y., Liu, C., Raj, A., Wieland, D. C. F., Garamus, V. M., Willumeit-Römer, R., Claesson, P. M. & Dėdinaitė, A. (2015). *J. Colloid Interface Sci.* **445**, 84–92.
Wieland, D. C. F., Degen, P., Zander, T., Gayer, S., Raj, A., An, J. X., Dėdinaitė, A., Claesson, P. & Willumeit-Römer, R. (2016). *Soft Matter*, **12**, 729–740.
Wieland, D. C. F., Garamus, V. M., Zander, T., Krywka, C., Wang, M., Dedinaite, A., Claesson, P. M. & Willumeit-Römer, R. (2016). *J. Synchrotron Rad.* **23**, 480–486.
Wirkert, F. J., Paulus, M., Nase, J., Möller, J., Kujawski, S., Sternemann, C. & Tolan, M. (2014). *J. Synchrotron Rad.* **21**, 76–81.
With, S., Trebbin, M., Bartz, C. B. A., Neuber, C., Dulle, M., Yu, S., Roth, S. V., Schmidt, H. W. & Förster, S. (2014). *Langmuir*, **30**, 12494–12502.
Yang, Z., Gu, Q. F., Lam, E., Tian, F., Chaieb, S. & Hemar, Y. (2016). *Food Hydrocolloids*, **56**, 58–61.
Zander, T., Wieland, D. C. F., Raj, A., Wang, M., Nowak, B., Krywka, C., Dėdinaitė, A., Claesson, P. M., Garamus, V. M., Schreyer, A. & Willumeit-Römer, R. (2016). *Colloids Surf. B*, **142**, 230–238.
Zappone, B., Ruths, M., Greene, G. W., Jay, G. D. & Israelachvili, J. N. (2007). *Biophys. J.* **92**, 1693–1708.